Periodic density-functional study on oxidation of diamond (100) surfaces

Periodic density-functional study on oxidation of diamond (100) surfaces

Hiroyuki Tamura, Hui Zhou, Kiyoshi Sugisako, Yasuto Yokoi, Seiichi Takami, Momoji Kubo, Kazuo Teraishi, and
Akira Miyamoto

Department of Materials Chemistry, Graduate School of Engineering, Tohoku University, Aoba-yama 07, Sendai 980-8579, Japan

Akira Imamura

Hiroshima Kokusai Gakuin University, 6-20-1, Aki-ku Nakano, Hiroshima City, 739-0321 Japan

Mikka N.-Gamo and Toshihiro Ando

National Institute for Research in Inorganic Materials, 1-1 Namiki, Tsukuba, Ibaraki 305 0044, Japan

(Received 28 July 1999)

The chemical reactions of the diamond surfaces with oxygen play important roles in the chemical-vapor deposition process, etching, and wear of the surface. In the present study, periodic density-functional calculations have been performed to clarify the oxidation mechanisms of the hydrogenated diamond (100) surfaces. The oxidation processes have been simulated in terms of the reaction heats. The ether, hydroxyl, and ketone structures are found to be stable on the diamond (100) surfaces. At the initial stage of the oxidation, the ether structures are priory formed at monohydride dimer bonds on the diamond (100) surfaces. The insertions of oxygen atoms into the lower layers are difficult to occur. As the coverage of oxygen atoms on the diamond surface is increased, the formation of ketone structures becomes easier. The stable structure of the oxygen monolayer sensitively depends on the lattice parameters. As the cell parameters are decreased, the bridge ether becomes more stable and the on-top ketone becomes more unstable.

I. INTRODUCTION

The chemical-vapor deposition (CVD) diamond thin films are potentially useful to various applications such as mechanical coatings, shaving tools, high-temperature semiconducting, heat sinks, optical electronics, electron emitters, and Schottky diodes. In order to realize a controllable process of the high-quality diamond growth, it is important to investigate a diamond growth mechanism from the gas phase. To elucidate this mechanism, it is important to understand the diamond surface structure and its chemistry because the diamond CVD growth proceeds on the surface. Generally, as-grown CVD diamond surfaces are terminated by hydrogen atoms.[1,2] For the diamond CVD growth from a gas phase, hydrogen is believed to play an important role in the maintenance of sp^3-bonded surfaces and the creation of surface radical sites.[3]

The structures and energetics of diamond surfaces have been studied both experimentally and theoretically. Hamza, Kubiak, and Stulen found 1×1 dihydride and 2×1 monohydride structures on the hydrogenated diamond (100) surfaces using low-energy electron diffraction (LEED).[2] Thoms and Butler also revealed using LEED and high-resolution electron-energy spectroscopies (HREELS) that the hydrogen is desorbed from the 2×1 monohydride above 1300 K and a clean 2×1 dimer row structure appeared.[4] The possible surface structures of the diamond (100), such as clean 2×1, 2×1 monohydride, and 1×1 dihydride, were exhaustively investigated by various theoretical methods such as empirical potential,[5,6] semiempirical,[7–9] or *ab initio*[10,11] molecular orbital (MO), quantum empirical combined molecular dynamics,[12] density-functional (DFT) calculations,[13–17] and tight-binding molecular dynamics (TBMD).[18,19] Hukka,

Pakkanen, and D'Evelyn calculated the heat of dehydrogenation of the monohydride and revealed that the second C-H dissociation of the dimer is easier than the first one due to the pairing of dangling bonds to form the π bond.[11] The equilibrium geometry and energetics of the diamond surfaces were studied, particularly, from the viewpoint of a comparison with those of Si.[20–22] As for the diamond (100) 2×1 clean surfaces, the higher-order reconstructions, which are observed for Si and Ge (100) due to buckling of surface dimer bonds, are not found. The 2×1 monohydride is believed to be the most stable state of the diamond (100), while the 1×1 dihydride is believed to be unstable due to steric repulsions between the hydrogen atoms.

In addition to hydrogen, it is also interesting to consider the role of oxygen in the diamond growth. It was reported that the addition of oxygen into the CVD plasma was supposed to enhance the diamond growth and improve the quality of the crystal.[23–28] In order to understand the role of oxygen on the diamond growth, the chemical reactions of oxygen containing species with diamond surfaces were investigated experimentally.[29–32] As the diamond surfaces are composed from carbon and hydrogen, the oxidation reactions are analogous to combustions of hydrocarbon molecules. Ando *et al.* investigated the chemical reaction of hydrogen and oxygen with diamond powders using Fourier-transform infrared (FTIR) and temperature programmed deposition (TPD) spectroscopies.[30,31] The chemisorbed species on the diamond surfaces were investigated as a function of the oxidation temperature, and various functional groups such as carbonyl (C=O), lactone [(C=O)O], carboxylic acid [(C=O)OH], cyclic ether (COC), and carboxylic anhydride [(C=O)O(C=O)] were found on the diamond surfaces.[31] The C-H bonds on the diamond surfaces were decreased and ether structures appeared on the diamond surfaces above 700 K, then at higher temperatures more carbonyl groups were

found. Finally, the oxygen-containing species were dissociated to desorb CO and CO_2 above 800 K. Pehrsson also observed the oxygen-containing species on the single-crystal diamond (100) surface using HREELS and revealed that at higher temperatures the C═O species preferentially desorb while the ether-bonded groups remain on the surface.[32]

The chemistry of the single-crystalline diamond surfaces is not so exhaustively studied compared with those of silicon, since the large area single crystals of diamond are difficult to obtain experimentally. Therefore, the details of the oxidation mechanism of the diamond surfaces are still open to debate although several experimental measurements have been performed. Theoretical study is expected to yield useful knowledge for understanding the oxidation mechanism of the diamond surfaces. In spite of its importance, there is only a handful of theoretical studies about the oxygenated diamond surfaces,[10,17,33–35] while the oxygenated silicon surfaces have been exhaustively studied both experimentally and theoretically. The difference in the oxidation processes between diamond and silicon crystals is also of interest to understand those solid-state properties. For instance, carbon has no stable bulk oxide phases, while silicon has various oxide structures. Understanding oxidation mechanisms are also important from the viewpoints of polishing, etching, and wear of the diamond surfaces. Moreover, the electronic properties of diamond, such as negative electron affinity[36] (NEA) and the Shottky barrier[37,38] are affected by the oxidation.

To investigate the structures and the energetics of the diamond surfaces particularly, the DFT calculations with the periodic boundary conditions are expected to be useful. Recent developments in *ab initio* molecular-dynamics methods[39] and pseudopotential concepts[40,41] reduced the computational costs in the DFT calculations and made them a practical tool in material science. In this study the periodic DFT calculations have been carried out to reveal the oxidation mechanisms of the diamond surfaces. The equilibrium geometries of the hydrogenated and the oxygenated diamond (100) surfaces have been calculated. The reaction paths of oxidation have been simulated in terms of the reaction heats.

II. METHODS

The periodic DFT calculations were performed using the CASTEP code, in which a plane-wave basis set and a conjugated gradient electronic minimization[42] are used. In the present study the electron-ion interactions are described using the norm-conserving nonlocal pseudopotentials[40] in real space.[41] The core radius [R_c (bohr)] of the carbon pseudopotential for each angular momentum is $R_c(s)=1.0$, $R_c(p)=1.4$, $R_c(d)=1.4$. The R_c of the oxygen pseudopotential used in the present calculations are 1.4 bohr for all of the angular momentum. The geometry optimizations are performed by the Broyden-Fletcher-Goldfarb-Shanno (BFGS) routine.[43] The exchange and correlation energies were calculated with the Perdew-Wang form of the generalized-gradient approximation (GGA).[44] The plane-wave cutoff energy was set at 1000 eV for all of the calculations. The above methods reproduce the lattice parameters of the diamond bulk crystal, which are only 1% smaller than the experimental values.

The supercell method was used to calculate the surface
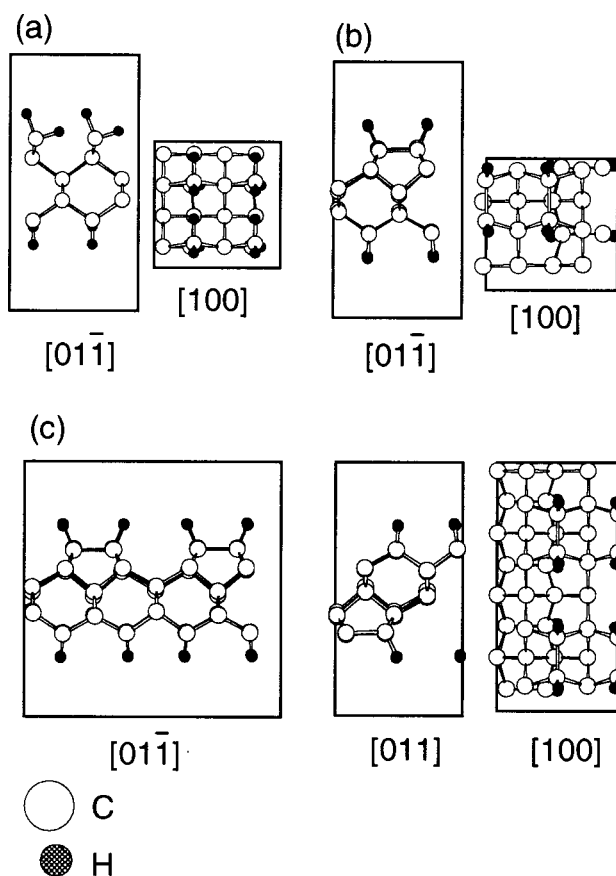
FIG. 1. Equilibrium geometries of the hydrogenated diamond (100) surfaces: (a) 1×1 dihydride and (b) 2×1 monohydride represented by the 2×2 supercell; (c) 2×1 monohydride represented by the 4×2 supercell.

and the molecular systems, where the crystal surface is represented by a finite-length slab and a molecule is put in a box and treated as a periodic system. Figure 1 shows the supercell models used in the calculations, where five layers of carbon atoms were extracted from the diamond crystal as a simple and efficient model to investigate the surface structures. The cell parameter along the [100] direction was set at 15 Å, which is long enough to avoid interactions between the replicas. As described later, the 2×1 monohydride structure [Fig. 1(b)] is much more stable than the 1×1 dihydride structure [Fig. 1(a)]. Therefore, the oxidation processes were investigated from the 2×1 structure and the bottom of the slab model was terminated by the 2×1 monohydrides. The 4×2 supercell [Fig. 1(c)] was also used to represent the longer periodic structures. In the present calculations, all of the cell parameters were fixed at the experimental value of the bulk crystal during the geometry optimizations while all of the atom positions were minimized with no symmetries. As the supercell for molecular systems, a 10-Å cubic box was used, where the molecule is regarded to be isolated in vacuum.

The reaction heat of the oxidation is defined as follows:

$$\Delta E = \Sigma E_{(\text{product})} - \Sigma E_{(\text{reactant})},$$

where ΔE is the reaction heat, $E_{(\text{product})}$ and $E_{(\text{reactant})}$ are the total energy of each product and reactant, respectively. According to the above definition, the positive and negative

TABLE I. Calculated structural parameters (in Å and degrees) of organic molecules and those of experimental values (Ref. 45).

		Structural parameters	
		Calc.	Expt.
H_2	H-H	0.75	0.74
O_2	O-O	1.14	1.21
H_2O	H-O	0.96	0.96
	$\angle HOH$	106	105
CO	C-O	1.10	1.13
CO_2	C-O	1.14	1.16
CH_4	C-H	1.09	1.09
C_2H_6	C-C	1.51	1.54
	C-H	1.09	1.09
	$\angle CCH$	112	111
C_2H_4	C-C	1.31	1.34
(ethylene)	C-H	1.08	1.09
	$\angle CCH$	122	121
$(CH_3)_2O$	C-O	1.40	1.42
(ether)	C-H	1.10	1.12
	$\angle COC$	113	112
CH_3OH	C-O	1.40	1.42
	C-H	1.10	1.09
	O-H	0.96	0.95
	$\angle COH$	110	109
$(CH_3)_2CO$	C=O	1.19	1.21
(acetone)	C-C	1.50	1.52
	C-H	1.09	1.10
	$\angle CCC$	117	116
C_2H_4O	C-C	1.45	1.47
(epoxy)	C-H	1.09	1.09
	C-O	1.40	1.43
	$\angle HCH$	115	116
	$\angle HCH-CC$ (out-of-plane)	157	158

TABLE II. Reaction heats of the vapor reaction of organic molecules from our calculations and experimental values (kcal/mol) (Ref. 46), where the number of oxygen atoms in the equations is equalized.

	Reaction heat	
Reaction	Calc.	Expt.
$2H_2+O_2=2H_2O$	-106	-116
$2CH_4=C_2H_6+H_2$	19	16
$C_2H_6=C_2H_4+H_2$	40	33
$2C_2H_6+O_2=2(CH_3)_2O$	-34	-48
$\frac{1}{2}CH_4+O_2=\frac{1}{2}CO_2+H_2O$	-83	-96
$\frac{2}{7}C_2H_6+O_2=\frac{4}{7}CO_2+\frac{6}{7}H_2O$	-84	-98
$\frac{1}{3}C_2H_4+O_2=\frac{2}{3}CO_2+\frac{2}{3}H_2O$	-94	-106
$\frac{1}{3}(CH_3)_2O+O_2=\frac{2}{3}CO_2+H_2O$	-93	-106
$\frac{2}{3}CH_3OH+O_2=\frac{2}{3}CO_2+\frac{4}{3}H_2O$	-95	-111
$\frac{1}{4}(CH_3)_2CO+O_2=\frac{3}{4}CO_2+\frac{3}{4}H_2O$	-89	-101
$\frac{2}{5}C_2H_4O+O_2=\frac{4}{5}CO_2+\frac{4}{5}H_2O$	-105	-116

The reaction heats of gas-phase reactions were calculated and compared with those of experimental values to check the reliability of the energetics. The experimental reaction heats were evaluated from the heat of formation of each molecule at room temperatures,[46] while our calculations did not take into account the temperatures and zero-point energies. In the cases of the oxidations of the organic molecules, the calculated reaction heats are systematically overestimated (i.e., less exothermic) than those of the experimental values (see Table II), where the number of oxygen in the equations is equalized. Since the bond length of O-O is especially underestimated, the systematic differences in the heats of oxidation seem to be mainly originated from the worst overestimation of the O-O bond energy. Considering this tendency, the calculated reaction heats of oxidations may be systematically overestimated.

values of ΔE mean endothermic and exothermic, respectively. As for the product and reactant, not only the hydrogenated and the oxygenated diamond slabs but also O_2, H_2, and H_2O molecules in the vapor phase were considered. The total spin of the oxygen molecule was set at 2 to assume the ground state.

III. RESULTS AND DISCUSSIONS

A. The equilibrium geometries and the reaction heats of organic molecules

The total energies of the O_2, H_2, and H_2O molecules at their equilibrium geometries were calculated to evaluate the reaction heats of oxidation. To confirm the accuracy of the calculations, the equilibrium geometries of other organic molecules were also calculated. The structural parameters of each molecule are summarized in Table I. The calculated structural parameters of the organic molecules are generally in agreement with the experimental values.[45] However, the bond lengths of C-C, C-O, and O-O tend to be underestimated. The differences between the calculations at 0 K and the experiments at room temperatures may contribute to this tendency.

B. The stable structure of hydrogenated diamond (100) surfaces

Figures 2(a) and 2(b) show the equilibrium geometries of the diamond (100) 1×1 dihydride and 2×1 monohydride, respectively. In the present calculations, the equilibrium C-C distance of the monohydride dimer is found to be 1.61 Å which is close to the result of the previous local-density approximation (LDA) calculations[16,22] (see Table III). For the diamond (100) 1×1 dihydride, the stability and equilibrium structures have been still the focus of the attentions.[6–9,12–14,16–20] In our GGA calculation, the dihydrides of the 1×1 state are found to be canted to avoid the steric repulsion between the hydrogen atoms. The canted dihydride is also found to be the most stable in the previous LDA calculations of the diamond (100) (Ref. 17) and Si (100).[47]

The reaction heat of the reconstruction from the 1×1 dihydride to the 2×1 monohydride with the desorption of the hydrogen molecules is found to be exothermic by Eq. (1) (see Table IV). Therefore, the 2×1 structures are more stable than the 1×1 structures considering the reaction with
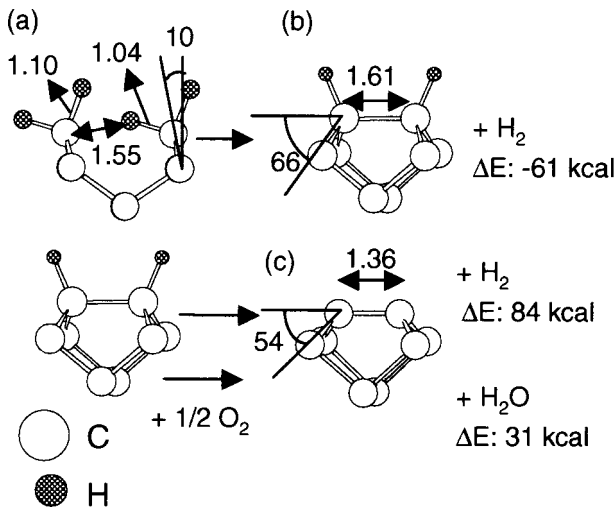
FIG. 2. Equilibrium geometries (in Å and degrees) of (a) 1×1 dihydride, (b) 2×1 monohydride, and (c) 2×1 clean dimer, where the geometries just around the dimer are shown.

the hydrogen molecules in the vapor phase. The 2×1 monohydride is considered to be the most favorable structure of the hydrogenated diamond (100) surfaces. In the following calculations, the diamond (100) surfaces are assumed to be terminated by the 2×1 monohydride before oxidation.

C. The desorption of hydrogen atoms from the monohydride

Figure 2(c) shows the equilibrium geometry of the 2×1 clean surface. The C-C distance of the dimer is decreased from those of the monohydride, as the charge density is transferred from the C-H bonds to the π bonding orbital at the dimer bond. The equilibrium C-C distance is found to be 1.36 Å, which is close to the results of the LDA calculations[15,16,21,22] (see Table III). The Jahn-Teller-like dis-

TABLE III. Calculated C-C length of clean and monohydride 2×1 dimers (in Å).

Reference No.	Clean	Monohydride
Present work (GGA)	1.36	1.61
5 (empirical)	1.38	1.63
6 (empirical)	1.46	1.63
7 (semiempirical)	1.43	1.67
8 (semiempirical)	1.58	1.73
9 (semiempirical)	1.38	1.56
11 (*ab initio*: MP2/6-31G*)		
constrained cluster	1.44	1.71
relaxed cluster	1.38	1.58
12 (semiempirical)	1.53	1.66
13 (LDA-TB)	1.40	1.67
14 (LDA-TB)	1.41	1.58
15 (LDA)	1.37	
16 (LDA)	1.37	1.61
18 (TB)	1.40	1.62
19 (TB)	1.54	
21 (LDA)	1.37	
22 (LDA)	1.38	1.62

tortion of dimers as observed on Si (100) ideal surfaces[20] were not found in the present calculations of diamond (100).

It is known that hydrogen is desorbed from the monohydride above 1300 K.[4,48] In the present calculation, the associative desorption of hydrogen from the monohydride is more endothermic by Eq. (2) in Table IV. The calculated heat of dehydrogenation of 84 kcal/mol quantitatively agrees with the activation energy of dehydrogenation obtained by TPD measurements of 80 kcal/mol.[48] Our calculation overestimates the reaction heat of H_2 desorption from C_2H_6 (see Table II) and so the heat of dehydrogenation of monohydride may be somewhat overestimated. The abstraction of the hydrogen atoms by oxygen molecules is also endothermic by Eq. (3) although the reaction is enhanced by the formation of H_2O molecules.

D. The formation of ether structures

Ether structures have been indicated on oxygenated diamond surfaces by IR spectra at the earlier stage of the oxidation.[31] In the present calculations, four different local minimum structures, which could be regarded as ether, were found after geometry optimizations from different initial guesses. The most stable site for ether formation is at the monohydride dimer bond [Fig. 3(a)], in which the C-C bond of the dimer is opened and a new C-O-C structure (namely an etherized dimer) is formed. The formation of the ether structure at the dimer bond is exothermic by Eq. (4). Therefore, the formation of ether at the monohydride is easier than the abstraction of hydrogen by oxygen. In the case of the insertion of the oxygen atom at the second layer [Fig. 3(b)], the distortion of the crystal structure is so large that the reaction with oxygen molecules is endothermic by Eq. (5). In the cases of the insertion of an oxygen atom at the third layer [Fig. 3(c) and 3(d)], the equilibrium geometries are more unstable than that at the second layer by Eqs. (6) and (7). According to these results, ether structures are priory formed at the dimer bonds of the diamond (100) surface while the insertion of oxygen atoms into the lower layers are more difficult.

Although the crystal structure of silicon is similar to those of diamond, the difference in the lattice parameters, elastic modulus, and ionicity seem to result in the different oxidation processes. In contrast to the diamond, previous experiments and DFT calculations revealed that the oxygen atoms can be easily inserted at the back bond of the Si (100) surface.[49,50] The MO calculations also revealed that the ionicity of the Si-O bonds enhance the oxidation into the lower layers.[51]

The 4×2 supercell was used for more precise modeling of the oxygenated diamond (100) surfaces. Figure 4(b) shows the equilibrium geometry of the etherized dimer which is surrounded by the other monohydride. The reaction heat to form this etherized dimer is found to be -31 kcal/mol, which is different from that of Fig. 3(a). To clarify the effect of arrangements of etherized dimers on their stabilities, the equilibrium geometries of two kinds of alignments were calculated. Figures 4(c) and 4(d) show the etherized dimers that aligned perpendicular and parallel to the dimer bonds, respectively. In the case of the perpendicular alignment [Fig. 4(c)], the reaction heat that forms the second ether is found to be -27 kcal/mol [Eq. (12) in Table V],

TABLE IV. Reaction heat (kcal/mol) of each reaction as shown in Figs. 2 and 3, which were calculated using a 2×2 supercell.

	ΔE	Eq.
Reconstruction from 1×1 dihydride to 2×1 monohydride		
Fig. 2(a)=Fig. 2(b)+H_2	-61	(1)
Desorption of hydrogen from monohydride		
Fig. (b)=Fig. 2(c)+H_2	84	(2)
Fig. 2(b)+$\frac{1}{2}O_2$=Fig. 2(c)+H_2O	31	(3)
Formation of ether		
at dimer Fig. 2(b)+$\frac{1}{2}O_2$=Fig. 3(a)	-18	(4)
at second layer Fig. 2(b)+$\frac{1}{2}O_2$=Fig. 3(b)	27	(5)
at third layer Fig. 2(b)+$\frac{1}{2}O_2$=Fig. 3(c)	54	(6)
Fig. 2(b)+$\frac{1}{2}O_2$=Fig. 3(d)	174	(7)
Formation of hydroxyl group		
first Fig. 2(c)+$\frac{1}{2}O_2$=Fig. 3(a)	-30	(8)
second Fig. 3(e)+$\frac{1}{2}O_2$=Fig. 3(g)	-42	(9)
Formation of ketone		
Fig. 2(b)+$\frac{1}{2}O_2$=Fig. 3(f)	-9	(10)

which is as large as the first ether formation. However, in the case of the parallel alignment [Fig. 4(d)], the reaction heat that forms the second ether is found to be -2 kcal/mol [Eq. (13)] which is less exothermic than that of the first ether formation. According to these results, the ether structures become more unstable when they are aligned parallel to the dimer bonds. This difference is caused by the steric repulsions between the hydrogen atoms from the etherized dimers, since the distance between the hydrogen atoms from the adjoined dimers is decreased by the insertion of the oxygen atoms at the dimer bonds.

E. The formation of hydroxyl groups

The hydroxyl groups were observed on the oxygenated diamond (100) surfaces in the IR (Ref. 28) and HREELS (Ref. 32) measurements. In the present calculations, the reaction heat that forms the hydroxyl group [Fig. 3(e)] is found to be -30 kcal/mol by Eq. (8), which is as large as that which forms the ether. The reaction heat of the formation of the second hydroxyl group [Fig. 3(g)] is found to be -42 kcal/mol by Eq. (9) which is larger than that which forms the first hydroxyl group due to the hydrogen bonding between the hydroxyl groups. A similar tendency was found in the previous MO calculations.[35] These results proved that the hydroxyl groups on the diamond (100) surface are thermodynamically stable. Actually, the activation energies may exist to form oxygenated structures such as ether and the hydroxyl groups.

F. Reaction paths that form ether and ketone structures

The IR spectra of the oxygenated diamond surfaces have indicated the C=O groups of ketone, lactone, carboxylic acid, and carboxylic anhydride.[31] Figure 3(f) shows the equilibrium geometry of the on-top ketone structure. The on-top ketone structure is found to be less stable than the bridge ether structure [Fig. 3(a)] although the stoichiometry is same.

These results indicate that the two C-O σ bonds are more favorable than one C=O double bond; in other words, the π bond is less favorable than the σ bond.

The reaction paths that form the ketone were investigated using the 4×2 supercell. The dissociations of two C-H bonds of the monohydride or the etherized dimer are necessary to form the ketone structure. The desorption of hydrogen from the monohydride with the formation of H_2O is found to be endothermic by Eq. (14); therefore, the clean 2×1 dimer is unstable intermediate to form ketone. Once the hydrogen is desorbed and the clean dimer is formed, the ketone structure as shown in Fig. 5(c) is spontaneously formed by adsorption of the oxygen molecules. The distance between two oxygen atoms from C=O groups is increased to 3.0 Å from the ideal C-C distance along the [011] direction (2.52 Å). The total reaction heat that forms the ketone structures from the monohydride with the desorption of H_2O molecules is found to be -100 kcal/mol [Eq. (14)+Eq. (17)]. However, according to the above reaction path, a ketone is more difficult to form than ether due to the unstable intermediate.

The reaction path to form the ketone from ether was also investigated. After the hydrogen atoms are removed from the etherized dimer, the C-C distance of the C-O-C structure is decreased and the equilibrium geometry, namely an epoxy structure, is found [Fig. 5(b)]. The desorption of hydrogen from the etherized dimer with the formation of H_2O is endothermic by Eq. (15); however, the energy to dissociate C-H bonds is lower than that from the monohydride dimer by 14 kcal/mol. When the epoxy structure is formed, the unsaturated carbon atoms are considered to be stabilized due to the formation of the new C-C bond. Once the hydrogen is desorbed and the epoxy structure is formed, the ketone structures are spontaneously formed by adsorption of the oxygen molecules. To form a ketone, the reaction path through the etherized dimer and the epoxy structure is more favorable than that through the clean 2×1 dimer.
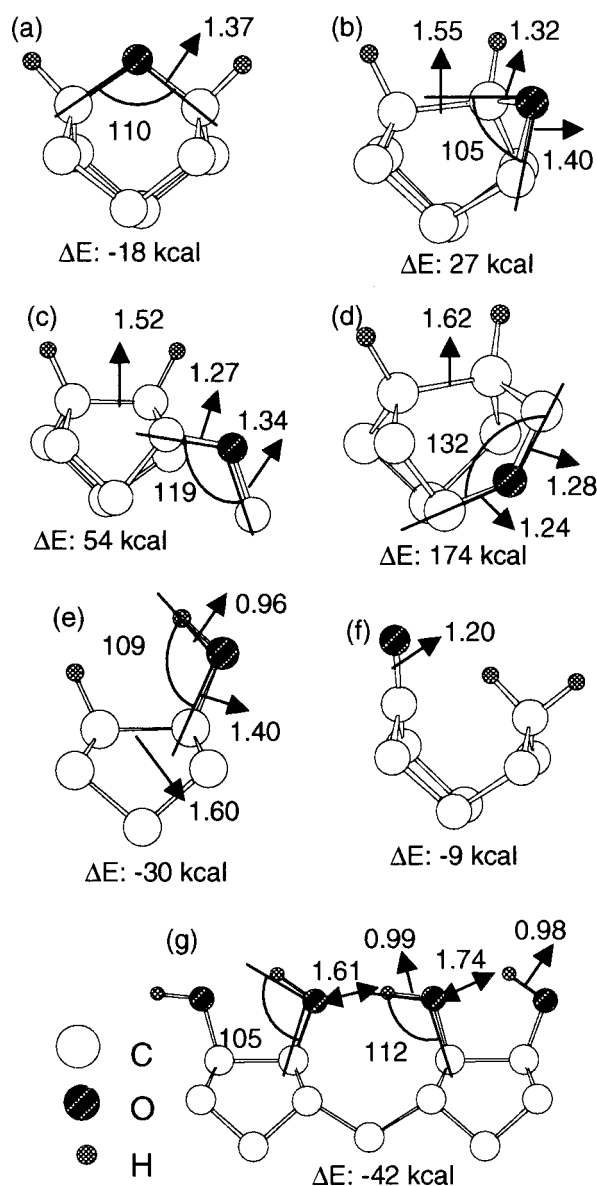
FIG. 3. Equilibrium geometries (in Å and degrees) of the ether structure (a) at the dimer bond; (b) at the second layer; (c) and (d) at the third layer; (e) hydroxyl group; and (f) ketone structure, where the geometries just around the dimer are shown. Equilibrium geometries of the aligned hydroxyl groups (g), where atoms in the replica cell are shown to indicate the O-H distance. ΔE indicates the reaction heat with $\frac{1}{2}$ O_2.

FIG. 4. Equilibrium geometries (Å) of the (a) 2×1 monohydride, (b) etherized dimer surrounded by other monohydrides, (c) etherized dimer aligned perpendicular to the dimer bonds, and (d) etherized dimer aligned parallel to the dimer bonds, where only the geometries of the upper layers are shown.

In the previous theoretical studies, two different opinions were found on the stable structures of C-O-C; one was the epoxylike closed dimer[33,34] and another was an opened C-O-C structure.[10,35] Skokov *et al.* mentioned that the calculation methods, which provide a relatively shorter C-C dimer length, tend to predict epoxylike closed C-O-C structures, and in the opposite cases opened C-O-C structures are found.[35] The C-C and C-O length tend to be underestimated in our calculations (see Table I) and so the epoxy structure more favorable agrees with the above idea.

If the etherized dimers are adjoined to each other parallel to the dimer bonds [Fig. 4(d)], the reaction heat to form the epoxy structure with the desorption of H_2O molecules is exothermic by Eq. (16). In the case of the reaction path follow-ing Eqs. (11), (13), (16), and (19), no unstable intermediates are found to form ketone. These results indicate that the formation of ketone structure is rather easy at the etherized dimer aligned parallel to the dimer bonds, since the desorption of hydrogen is easier due to the repulsion between the hydrogen atoms.

The reaction heat to dissociate two C-H bonds from the neighboring different etherized dimers is found to be 0 kcal/mol by Eq. (20). Once the hydrogen is desorbed, the formation of the bridging ether as shown in Fig. 6(d) is found to be exothermic by Eq. (21). Therefore, to form the bridge ether, no unstable intermediates exist. The three chains of bridge ether are more stable than two ketone and one ether structures [Fig. 6(b)] although the stoichiometry is the same. This difference is caused by the difference in the stability between the π bond and the σ bond as mentioned above.

Our calculations predict the reaction paths of the oxidation of the diamond (100) as follows. At the initial stage of the oxidation, the formation of ether structures at dimer bonds is more favorable than the formation of the ketone structures. Then, as the density of the etherized dimer is increased, the desorption of hydrogen, and therefore the formation of the ketone structures, becomes easier. To investi-

TABLE V. Reaction heat (kcal/mol) of each reaction as shown in Figs. 4, 5, and 6, which were calculated using a 4×2 supercell.

		ΔE	Eq.
Formation of the first ether			
	Fig. 4(a)$+\frac{1}{2}O_2=$Fig. 4(b)	-31	(11)
Formation of the second ether			
perpendicular	Fig. 4(a)$+\frac{1}{2}O_2=$Fig. 4(c)	-27	(12)
parallel	Fig. 4(a)$+\frac{1}{2}O_2=$Fig. 4(d)	-2	(13)
Desorption of hydrogen from monohydride			
	Fig. 4(a)$+\frac{1}{2}O_2=$Fig. 5(a)$+H_2O$	29	(14)
Desorption of hydrogen from etherized dimer			
	Fig. 4(b)$+\frac{1}{2}O_2=$Fig. 5(b)$+H_2O$	15	(15)
	Fig. 4(c)$+\frac{1}{2}O_2=$Fig. 6(a)$+H_2O$	-17	(16)
Formation of ketone			
from clean dimer	Fig. 5(a)$+O_2=$Fig. 5(c)	-129	(17)
from epoxy	Fig. 5(c)$+\frac{1}{2}O_2=$Fig. 5(c)	-84	(18)
	Fig. 6(a)$+\frac{1}{2}O_2=$Fig. 6(b)	-61	(19)
Desorption of hydrogen from adjoined etherized dimers			
	Fig. 4(c)$+\frac{1}{2}O_2=$Fig. 6(c)$+H_2O$	0	(20)
Formation of three chains of ether			
	Fig. 6(c)$+\frac{1}{2}O_2=$Fig. 6(d)	-92	(21)

gate more exactly, the activation energies and the effect of temperatures must be taken into account. In the IR measurements of the oxygenated diamond powders, also more C=O groups are found as the oxidation goes on.[31] In the HREELS study of the oxygenated diamond (100), the desorption of C=O is found to be easier than that of C-O-C and so the ether/ketone ratio increases at higher oxygen coverage.[32] Therefore, the desorption of oxygen-containing species must be also considered to elucidate the oxidation mechanisms of diamond surfaces.

G. Full coverage oxygen monolayer

Thomas Rudder, and Markunas revealed by LEED patterns that atomic oxygen readily converts the diamond (100) from the 2×1 state of the 1×1 state.[29] Hamza, Kubiak, and Stulen also mentioned that the 1×1 states were observed on the annealed diamond (100) surfaces when oxygen existed.[2] Two configurations are considered for the oxygenated 1×1 states: one is the bridge ether type and another is the on-top ketone type. Skokov, Weiner, and Frenklach performed the semiempirical molecular dynamics and found that the on-top ketone structure becomes more stable as the temperature becomes higher due to an increase in entropy.[35] In the LDA calculations of the oxygenated diamond (100) performed by Rutter and Robertson, the bridge ether is found to be more stable than the on-top ketone.[17] The ketone structures are considered to be peculiar to carbon; therefore, for Si (100) surfaces different features are observed although their crystal structures are similar to those of the diamond. As for the oxygenated Si (100) surfaces, a 1×1 LEED pattern is observed when the oxygen atoms are fully covered.[54] The MO (Ref. 52) and DFT (Ref. 53) calculations revealed that the bridging Si-O-Si structure is the most favorable for the 1×1 oxygenated Si (100) surfaces.

In our calculations of the 1×1 oxygenated diamond (100), even if the geometry optimization is started from the
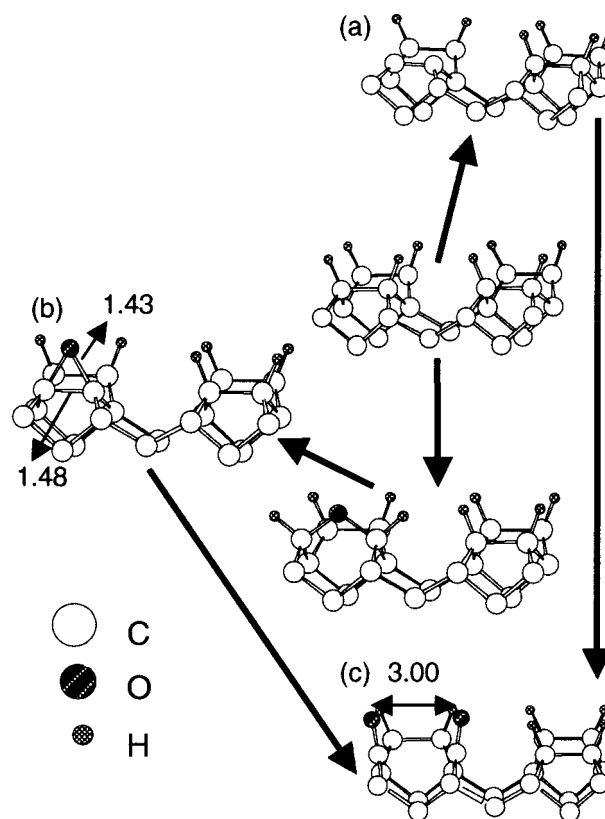
FIG. 5. Equilibrium geometries (Å) of the (a) 2×1 clean dimer surrounded by other monohydrides, (b) epoxylike C-O-C structure, and (c) ketone structures, where only the geometries of the upper layers are shown. The bold arrows indicate the reaction paths to form the ketone.
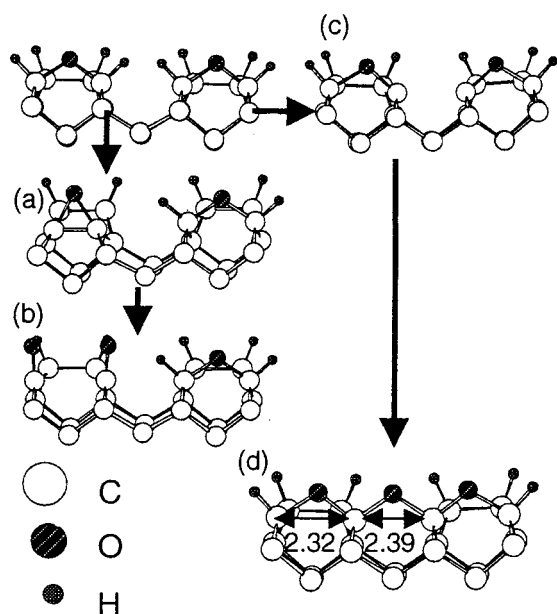
FIG. 6. Reaction paths to form the ketone from the parallel aligned ether, where the equilibrium geometries of the upper layers are shown (Å): (a) the hydrogen atoms are dissociated and the epoxy is formed; (b) the ketone structures are formed; (c) the hydrogen atoms are dissociated from the adjoined etherized dimers; (d) the bridging ether structures.

bridge ether structure [Fig. 7(a)], the on-top ketone structure [Fig. 7(b)] is obtained. The reason can be explained by the difference in the equilibrium C-C distance of molecular ethers and those of diamond (100) surfaces. The equilibrium C-C distance stride across the oxygen atom of ether molecules (2.30 Å) is shorter than the C-C distance along the [011] direction of the diamond crystals (2.52 Å). In the case of the 1×1 bridge ether structure, the C-O-C structures are unnaturally stretched. Therefore, they are found to be less stable than the ketone structures although the σ bonds of C-O-C are more stable than the π bonds of C=O. In the case of three chains of the C-O-C structure [Fig. 6 (d)], the C-C
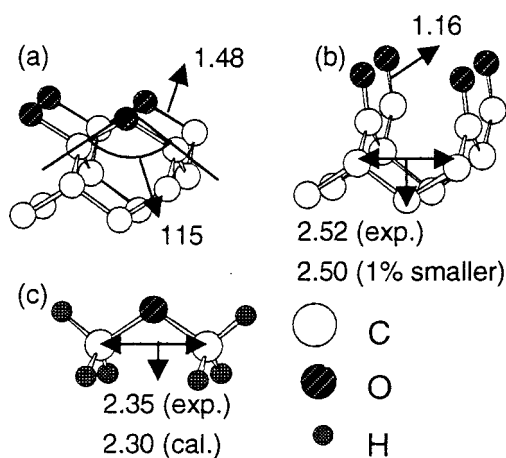
TABLE VI. Relative stability of the bridge ether and on-top ketone structures of the oxygen monolayers, where the values indicate the difference in the total energies from the 1% smaller bridge ether (kcal/mol).

C-C distance along [110] (Å)	Bridge ether	On-top ketone
2.52 (Experimental value)	Unstable	+8
2.50 (1% smaller)	0	+11

distances are decreased from the ideal position of the diamond crystal and so the ether structures are stabilized. It is predicted that the C-O-C structures become more unstable as they are continued longer. In the above calculations the lattice parameters were fixed at the experimental values although the C-C and C-O bond lengths tend to be underestimated. To verify the results, the stabilities of the bridge ether and the on-top ketone were investigated using 1% smaller lattice parameters. In the case of the 1% smaller lattice parameters, the bridge ether is stabilized while the on-top ketone became more unstable due to an increase of repulsions between the C=O groups. Therefore, the bridge ether is found to be more stable than the on-top ketone (Table VI). These results indicate that the relative stability between the bridge ether and the on-top ketone is sensitive to the lattice parameters. As the lattice parameters are decreased, the bridge ether structures become more favorable than the on-top ketone structures.

IV. CONCLUSIONS

In the present study, the oxidation processes of diamond (100) surfaces were investigated by the periodic DFT calculations using the norm-conserving pseudopotentials and the generalized gradient approximation. Ether, hydroxyl, and ketone structures are found to be stable on the diamond (100) surfaces. The formation of ether at the monohydride dimer bond is much easier than either the oxidation into lower layers or the desorption of hydrogen from the monohydride. The on-top ketone structure is less stable than the ether structure at the initial stage of the oxidation.

The desorption of hydrogen from the etherized dimer is easier than that from the monohydride, especially when the etherized dimers are adjoined parallel to the dimer bonds; the desorption of hydrogen is found to be exothermic. To form a ketone, the reaction path through the etherized dimer and the epoxy structure is more favorable than that through the clean 2×1 dimer.

The stable structure of the 1×1 oxygen monolayer sensitively depends on the lattice parameters. In the case of the experimental lattice parameter, the on-top ketone is found to be more stable than the bridge ether. This tendency is explained by the fact that the longer C-C distance of the diamond (100) surface stretches the C-O-C structures and makes them unstable. As the cell parameters are decreased, the bridge ether becomes more stable and the on-top ketone becomes more unstable.

Our calculations predict that the ether structures are expected to be priory formed at the initial stage of the oxidation of diamond (100), then the formation of the ketone structures becomes easier as the coverage of oxygen is increased.

FIG. 7. Equilibrium geometries (in Å and degrees) of the full coverage oxygen monolayers, where the C-C distance along the [011] direction from experiment is 2.52 Å and the 1% shorter one is 2.50 Å: (a) the bridge ether and (b) the on-top ketone calculated using the 1% smaller cell; (c) the C-C distance of ether molecules.

[1] F. G. Celii and J. E. Butler, Annu. Rev. Phys. Chem. **42**, 643 (1991).

[2] A. V. Hamza, G. D. Kubiak, and R. H. Stulen, Surf. Sci. **237**, 35 (1990).

[3] B. B. Pate, Surf. Sci. **165**, 83 (1986).

[4] B. D. Thoms and J. E. Butler, Surf. Sci. **328**, 291 (1995).

[5] D. W. Brenner, Phys. Rev. B **42**, 9458 (1990).

[6] Y. L. Yang, M. P. D'Evelyn, J. Am. Chem. Soc. **114**, 2796 (1992); J. Vac. Sci. Technol. A **10**, 978 (1992).

[7] W. S. Verwoerd, Surf. Sci. **103**, 404 (1981); **108**, 153 (1981).

[8] S. P. Mehandru and A. B. Anderson, Surf. Sci. **248**, 369 (1991).

[9] X. M. Zheng and P. V. Smith, Surf. Sci. **256**, 1 (1991).

[10] J. L. Whitten and P. Cremaschi, Appl. Surf. Sci. **75**, 45 (1994).

[11] T. I. Hukka, T. A. Pakkanen, and M. P. D'Evelyn, J. Phys. Chem. **98**, 12 420 (1994).

[12] S. Skokov, C. S. Carmer, B. Weiner, and M. Frenklach, Phys. Rev. B **49**, 5662 (1994).

[13] S. H. Yang, D. A. Drabold, and J. B. Adams, Phys. Rev. B **48**, 5261 (1993).

[14] Th. Frauenheim, U. Stephan, P. Blaudeck, D. Porezag, H.-G. Busmann, W. Zimmermann-Edling, and S. Lauer, Phys. Rev. B **48**, 18 189 (1993).

[15] C. Kress, M. Fiedler, W. G. Schmidt, and F. Bechstedt, Phys. Rev. B **50**, 17 697 (1994).

[16] J. Furthmüller, J. Hafner, and G. Kresse, Phys. Rev. B **50**, 15 606 (1994); **53**, 7334 (1996).

[17] M. J. Rutter and J. Robertson, Phys. Rev. B **57**, 9241 (1998).

[18] B. N. Davidson and W. E. Pickett, Phys. Rev. B **49**, 11 253 (1994).

[19] M. D. Winn, M. Rassinger, and J. Hafner, Phys. Rev. B **55**, 5364 (1997).

[20] F. Bechstedt and D. Reichardt, Surf. Sci. **202**, 83 (1988).

[21] P. Krüger and J. Pollmann, Phys. Rev. Lett. **74**, 1155 (1995).

[22] T. Ogitsu, T. Miyazaki, M. Fujita, and M. Okazaki, Phys. Rev. Lett. **75**, 4226 (1995).

[23] Y. Hirose and Y. Terasawa, Jpn. J. Appl. Phys., Part 1 **25**, L519 (1986).

[24] T. Kawato and K. Kondo, Jpn. J. Appl. Phys., Part 1 **26**, 1429 (1987).

[25] Y. Saito, K. Sato, H. Tanaka, K. Fujita, and S. Matuda, J. Mater. Sci. **23**, 842 (1988).

[26] Y. Liou, R. Weimer, D. Knight, and R. Messier, Appl. Phys. Lett. **56**, 437 (1990).

[27] Y. Muranaka, H. Yamashita, and H. Miyadera, J. Appl. Phys. **69**, 8145 (1991).

[28] L. M. Struck and M. P. D'Evelyn, J. Vac. Sci. Technol. A **11**, 1992 (1993).

[29] R. E. Thomas, R. A. Rudder, and R. J. Markunas, J. Vac. Sci. Technol. A **10**, 2451 (1992).

[30] T. Ando, M. Ishii, M. Kamo, and Y. Sato, J. Chem. Soc., Faraday Trans. **89**, 1783 (1993).

[31] T. Ando, K. Yamamoto, M. Ishii, M. Kamo, and Y. Sato, J. Chem. Soc., Faraday Trans. **89**, 3635 (1993).

[32] P. E. Pehrsson, Electrochem. Soc. Proc. **95-4**, 436 (1995).

[33] P. Badziag and W. S. Verwoerd, Surf. Sci. **183**, 469 (1987).

[34] X. M. Zheng and P. V. Smith, Surf. Sci. **262**, 219 (1992).

[35] S. Skokov, B. Weiner, and M. Frenklach, Phys. Rev. B **49**, 11 374 (1994); **55**, 1895 (1997).

[36] N. Eimori, Y. Mori, A. Hatta, T. Ito, and A. Hiraki, Jpn. J. Appl. Phys., Part 1 **33**, 6312 (1994).

[37] Y. Mori, H. Kawarada, and A. Hiraki, Appl. Phys. Lett. **58**, 940 (1991).

[38] H. Kiyota, E. Matsushima, K. Sato, H. Okushi, T. Ando, M. Kamo, Y. Sato, and M. Iida, Appl. Phys. Lett. **67**, 3596 (1995).

[39] R. Car and M. Parrinello, Phys. Rev. Lett. **55**, 2471 (1985).

[40] D. R. Hamann, M. Schlüter, and C. Chiang, Phys. Rev. Lett. **43**, 1494 (1979); G. B. Bachelet, D. R. Hamann, and M. Schlüter, Phys. Rev. B **26**, 4199 (1982).

[41] R. D. King-Smith, M. C. Payne, and J. S. Lin, Phys. Rev. B **44**, 13 063 (1991).

[42] M. P. Teter, M. C. Payne, and D. C. Allan, Phys. Rev. B **40**, 12 255 (1989).

[43] E. Polak, *Computational Methods in Optimization* (Academic, New York, 1971), p. 56ff.

[44] K. Burke, J. P. Perdew, and M. Levy, *Modern Density Functional Theory: A Tool for Chemistry*, edited by J. M. Seminario and P. Politzer Theoretical and Computational Chemistry Vol. 2 (Elsevier, New York, 1995), pp. 29–74.

[45] L. E. Sutton, *Tables of Interatomic Distance and Configuration in Molecules and Ions*, The Chemical Society Spatial Publication No. 11 (The Chemical Society, London, 1958), and *ibid.*, Spatial Publication No. 18 (1965).

[46] J. B. Pedley and J. Rylance, *Computer Analyzed Thermochemical Data: Organic and Organometallic Compounds* (University of Sussex, Sussex, England, 1977).

[47] J. E. Northrup, Phys. Rev. B **44**, 1419 (1991).

[48] C. Su and J. C. Lin, Surf. Sci. **406**, 149 (1998).

[49] H. Watanabe, K. Kato, T. Uda, K. Fujita, M. Ichikawa, T. Kawamura, and K. Terakura, Phys. Rev. Lett. **80**, 345 (1998).

[50] K. Kato, T. Uda, and K. Terakura, Phys. Rev. Lett. **80**, 2000 (1998).

[51] K. Teraishi, H. Takaba, A. Yamada, A. Endou, I. Gunji, A. Chatterjee, M. Kubo, A. Miyamoto, K. Nakamura, and M. Kitajima, J. Chem. Phys. **109**, 1495 (1998).

[52] P. V. Smith and A. Wander, Surf. Sci. **219**, 77 (1989).

[53] Y. Miyamoto and A. Oshiyama, Phys. Rev. B **41**, 12 680 (1990).

[54] E. G. Keim, L. Wolterbeek, and A. V. Silfhout, Surf. Sci. **180**, 565 (1987).